

We are IntechOpen, the world's leading publisher of Open Access books Built by scientists, for scientists

5,800

Open access books available

142,000

International authors and editors

180M

Downloads

Our authors are among the

154

Countries delivered to

TOP 1%

most cited scientists

12.2%

Contributors from top 500 universities



WEB OF SCIENCE™

Selection of our books indexed in the Book Citation Index
in Web of Science™ Core Collection (BKCI)

Interested in publishing with us?
Contact book.department@intechopen.com

Numbers displayed above are based on latest data collected.
For more information visit www.intechopen.com



Analysis and Design of Absorbers for Electromagnetic Compatibility Applications

Shiva Hayati Raad

Abstract

Absorbers are one of the key components in the realm of electromagnetic compatibility. Depending on the frequency range of interest, different types of absorbers can be utilized for this purpose. This chapter introduces the analysis and modeling of ferrite-based absorbers for low-frequency applications (below 1 GHz) and discusses the issues encountered in their installation, resulting in air gaps. Later, different kinds of pyramidal absorbers, commonly used in the broadband microwave frequency range (above 1 GHz), are presented, and analytical and numerical approaches for predicting their performance are reviewed. The combination of the ferrite tile and pyramidal dielectric absorbers is also provided. Then, some practical aspects of designing hybrid absorbers, including the influence of carbon loading and matching layer on their performance, are mentioned. Finally, the absorber operating frequency extension to the millimeter-wave spectrum using metamaterial structures or graphene material is presented.

Keywords: ferrite absorber, dielectric absorber, hybrid absorber, matching layer, air gaps, absorber modeling, millimeter-wave

1. Introduction

The electromagnetic compatibility of the electronic devices is mainly considered in two ways, measuring radiated emission (RE) or radiated immunity (RI), where the test procedures are specified in different standards [1, 2]. The frequency spectrum of RE/RI tests starts from tens of kHz. Since the absorber technology cannot cover such low frequencies, the concentration of the absorber design goes around 70 MHz test frequencies [3]. Anechoic chambers (AC) in the form of fully or partially covered rooms with electromagnetic absorbers that simulate the open area test site (OATS) are the most common indoor facilities for the electromagnetic compatibility (EMC) tests, where the quality of the installed absorbers influences the precision of the tests [4]. Moreover, there are other types of shielded enclosures such as compact renege rooms, transverse electromagnetic (TEM) cells, and gigahertz transverse electromagnetic (GTEM) cells. Properly lining these test facilities with absorbing materials is a key factor for their expected operation [5–8].

When an electromagnetic wave illuminates an environment, it is reflected, transmitted, or absorbed. An efficient absorber can be realized by minimizing the contributions of the former two components [9]. For covering the test frequencies

in different applications, broadband absorbers are necessary. Various approaches are proposed for bandwidth enhancement of the electromagnetic absorbers, multi-resonance and multilayered structures being two important groups, realized by merging multiple closely spaced resonances [10, 11]. Broadband absorbers in the EMC field are commonly attained by tapered geometries, such as wedge or pyramidal configurations, or by parameter gradient flat structures to provide gradual impedance matching [12]. In all cases, the metallic backside prevents wave transmission [5]. Unit cell analysis, transmission-line model, homogenization method, finite difference time domain (FDTD) technique, and mode-matching technique are some of the approaches that have been used for the performance prediction of the absorbers [13–18]. In this chapter, the analysis and design of some important types of EMC absorbers are reviewed. The chapter also includes millimeter-wave absorbers for future EMC applications.

2. Analysis and design of absorbers for the electromagnetic compatibility applications

Different types of absorbing materials and geometries are used for EMC applications depending on the operating frequency range. Below 1 GHz, ferrite-based materials having dispersive lossy permeability are used in different planar configurations. Moreover, above 1 GHz, electric losses or magnetic losses provided by lossy dielectric or lossy magnetic materials, respectively, can be used. To cover both of the above ranges, hybrid absorbers constructed by combining the ferrite tiles and pyramidal absorbers are a solution. In the higher microwave/THz frequencies, metamaterial absorbers can be used. In the following subsections, a detailed discussion of each category is presented. Note that the required absorber's reflectivity is dedicated by the frequency range and its application. Specifically, the military standard requires -6 dB normal incidence reflectivity for 50–250 MHz frequencies and -10 dB normal incidence reflectivity above 250 MHz. Moreover, for immunity tests, -18 dB normal incidence reflectivity for 80–1000 MHz spectrum is essential. For emission tests in 3-meter chambers, -18 dB normal incidence reflectivity for 30–1000 MHz region and -12 dB at 45° for 30–1000 MHz spectrum fulfill the requirements, while in 10-meter chambers, -20 dB normal incidence reflectivity for 30–1000 MHz spectrum and -15 dB at 45° for 30–1000 MHz range are required [19]. Typical reflectivity of absorbers in different frequency bands can be found in the data sheets provided by the manufacturers, from which an appropriate absorber model can be specified. **Table 1** is given as an example [20]. Finally, depending on the operating frequency range, NRI arch, waveguide, coaxial line, time-domain method, and free-space approach can be used for the performance evaluation of the absorbers [17, 21]. The test procedures are specified in IEEE Standard 1128 [22]. The difference between measured reflection coefficient (S_{11}) with and without the absorber is the reflectivity in the former method. In the latter approach, reflectivity is attained by comparing the received power with that using the perfect electric conductor (PEC) plate [20, 23].

2.1 Ferrite absorbers

The simplest type of ferrite absorbers is ferrite tiles, where the whole desired surface can be covered by installing multiple tiles next to each other. This type of absorber is shown in **Figure 1(a)**, backed by a PEC layer. Ferrite tile ceramics are realized by heating powders under pressure at 1000–1500°C. Thus, brittle and thin tiles between 4 and 7 mm are commonly used because of the heavyweight of iron,

Model number	80 MHz	120 MHz	200 MHz	300 MHz	500 MHz	L-BAND 1–2 GHz	S-BAND 2–4 GHz	C-BAND 4–8 GHz	X-BAND 8–12 GHz	KU-BAND 12–18 GHz	K-BAND 18–40 GHz
EHP-3PCL								–30 dB	–40 dB	–45 dB	–45 dB
EHP-5PCL							–30 dB	–40 dB	–45 dB	–50 dB	–50 dB
EHP-8PCL						–30 dB	–40 dB	–45 dB	–50 dB	–50 dB	–50 dB
EHP-12PCL						–35 dB	–40 dB	–45 dB	–50 dB	–50 dB	–50 dB
EHP-18PCL					–30 dB	–40 dB	–45 dB	–50 dB	–50 dB	–50 dB	–50 dB
EHP-24PCL			–20 dB	–30 dB	–35 dB	–40 dB	–50 dB	–50 dB	–50 dB	–50 dB	–50 dB
EHP-36PCL	–11 dB	–13 dB	–25 dB	–30 dB	–40 dB	–45 dB	–50 dB	–50 dB	–50 dB	–50 dB	–50 dB
EHP-48PCL	–15 dB	–20 dB	–30 dB	–35 dB	–40 dB	–45 dB	–50 dB	–50 dB	–50 dB	–50 dB	–50 dB
EHP-72PCL	–20 dB	–30 dB	–40 dB	–40 dB	–45 dB	–50 dB	–50 dB	–50 dB	–50 dB	–50 dB	–50 dB
EMC-24PCL	–6 dB	–6 dB	–7 dB	–30 dB	–35 dB	–45 dB	–50 dB	–50 dB	–50 dB	–50 dB	–45 dB

Table used with permission of ETS-Lindgren.

Table 1.
Typical reflectivity of a specific absorber series in different frequency bands for normal incidence [20].

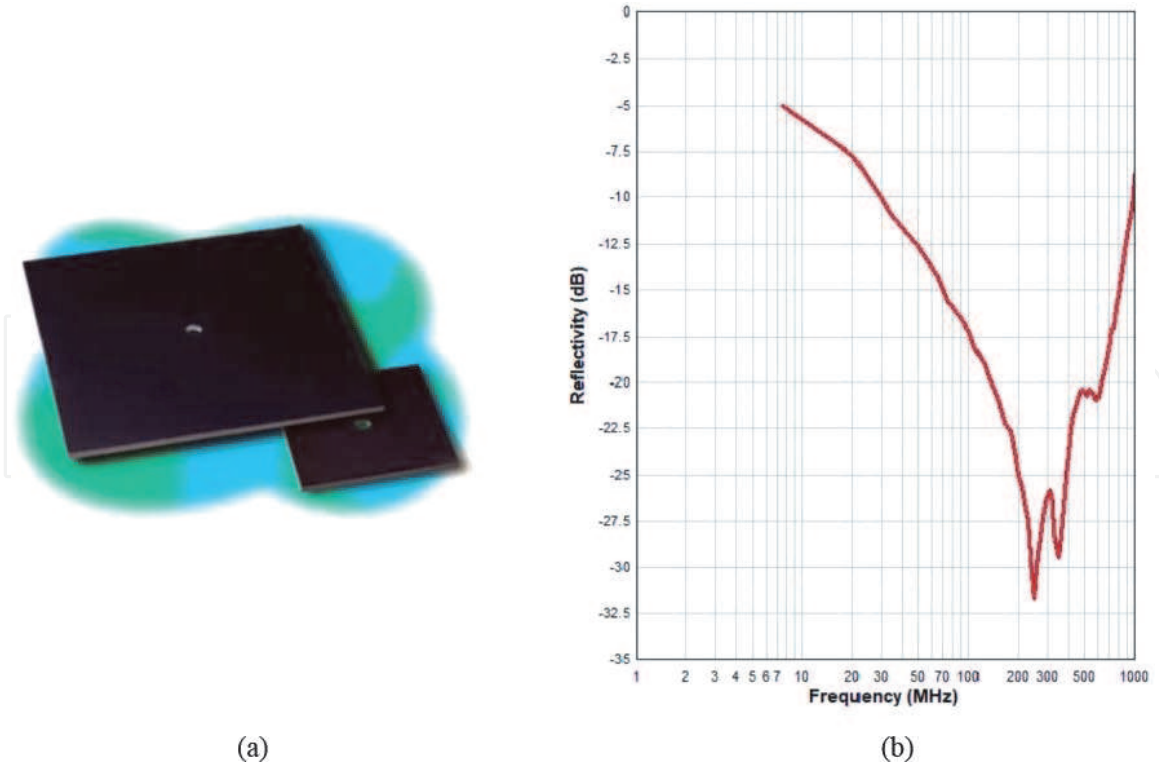


Figure 1. (a) Ferrite tile absorber [24] and (b) its typical reflectivity [25] (The photos used with permission of ETS-Lindgren).

manganese, and other metal oxides [1]. The typical surface area of the tiles is 100 mm^2 , and they are usually installed onto plywood panels leading to an extremely fire-retardant installation [5]. Due to the low operation frequency, the homogenization of the entire structure and later using the transmission line method gives reasonable results for the associated absorption rate. Thus, the surface impedance of the shortened ferrite slab is [14]:

$$\eta_t = \eta_0 \sqrt{\frac{\mu_r}{\epsilon_r}} \tanh\left(\frac{2\pi t}{\lambda_0} \sqrt{\mu_r \epsilon_r}\right) \quad (1)$$

where t is the thickness of the tile, η_0 is the free-space intrinsic wave impedance, $\epsilon_r = 14$ is the relative permittivity of the tile, and μ_r is the relative permeability calculated by the Drude model, which reads as [26]:

$$\mu_r = 1 + \frac{1101.4}{1 + j \frac{f}{7.066 \times 10^6}} \quad (2)$$

where f is the operating frequency. Using the aforesaid surface impedance, the reflectivity of the ferrite tile absorbers can be calculated readily. **Figure 1(b)** shows the typical reflectivity of a ferrite tile.

An inherent problem of installing the ferrite tiles is the small-sized air gaps between the adjacent cells. The air gaps result in performance degradation due to the significant difference between the permeability of the air gaps and ferrite material. The impact of air gaps on the performance of the ferrite tile absorbers can be approximated *via* their similarity to the air gaps in the core of power transformers to obtain the equivalent permeability as [14]:

$$\mu_r^e = \frac{\mu_r}{1 + \frac{\Delta}{t} (\mu_r - \mu_{air})} \quad (3)$$

Maxwell Garnett formula	$\mu_{eff} = \mu_b \left[1 + \frac{2g(\mu_i - \mu_b)}{(1-g)\mu_i + (1+g)\mu_b} \right]$
Bruggeman formula	$(1-g) \frac{\mu_b - \mu_{eff}}{\mu_b + \mu_{eff}} + g \frac{\mu_i - \mu_{eff}}{\mu_i + \mu_{eff}} = 0$
Liu formula	$\mu_{eff} = \frac{\mu_i}{1 + (1 - \sqrt{g}) \left(\frac{\mu_i}{\mu_b} - 1 \right)}$
Hashin–Shtrikman bounds	$\mu_b \frac{(1-g)\mu_b + (1+g)\mu_i}{(1+g)\mu_b + (1-g)\mu_i} \leq \mu_{eff} \leq \frac{(2-g)\mu_b + g\mu_i}{g\mu_b + (2-g)\mu_i} \mu_i$

Table 2.
 Different homogenization approaches for modeling ferrite tiles with air gaps [29].

where Δ is the size of the air gap perpendicular to the magnetic field and l is the width of the ferrite tile. Some gap-filling materials, such as ferrite rubber or developed plastic material called REC 65, are proposed to obviate this issue [27]. Moreover, ferrite absorbers are fabricated in other geometries such as grids, where they have an additional degree of freedom to adjust the resonant frequency through the filling factor. Therefore, synthesized capacitance and synthesized inductance models can be used to determine the effective permeability of the ferrite grids and ferrite grids with air gaps [28]. Furthermore, due to the lower amount of utilized ferrite material in the fabrication, the performance sensitivity to the air gaps is lower in the ferrite grids with respect to the ferrite tiles. Different homogenization approaches for modeling ferrite tiles with air gaps are summarized in **Table 2**. Note that these approximate mixing rules do not always work well, especially for hollow and wedge shapes (or other complicated shapes). A full numerical model using a unit cell/periodic boundary (Floquet ports) and full-wave modeling is fast and easy. The full-wave model can account for air gaps and complicated shapes [29]. As a final comment, due to ferrite tile's heavyweight and expensive cost, its minimum usage, which is predicted by the optimization tools, is preferred [30–32].

2.2 Pyramidal absorbers

Different types of dielectric absorbers having lossy permittivity (electric loss) or permeability (magnetic loss) are commonly used for the wideband electromagnetic wave absorption above 1 GHz [5]. Organic materials (such as rice straw, oil palm empty fruit bunch, sugar cane bagasse, and coconut shell [33]), magnetic materials (such as NiZn spinel ferrite, Co₂Z hexaferrite, and RuCoM hexaferrite [34]), and dielectric materials (such as foam (carbon-based), polyurethane, polystyrene, polyethylene, and thin film [30]) can be used for this purpose. The absorption capability of each material can be evaluated using its constitutive parameters. To this end, the attenuation constant of the incoming wave is calculated to guarantee that the wave can penetrate the device. Therefore [2],

$$\alpha = \omega \sqrt{\epsilon_0 \mu_0} (a^2 + b^2)^{1/4} \sin \left(\frac{1}{2} \tan^{-1} \left(\frac{a}{b} \right) \right) \quad (4)$$

where prime and double prime, respectively, denote the real and imaginary parts of the permittivity (ϵ) and permeability (μ). Also, the parameters a and b in Eq. (4) are defined as follows:

$$a = (\epsilon'_r \mu'_r - \epsilon''_r \mu''_r) \quad (5)$$

$$b = (\epsilon'_r \mu''_r + \epsilon''_r \mu'_r) \quad (6)$$

Note that the real and imaginary parts of the constitutive parameters cannot change arbitrarily, and the Kramers–Kronig relationship should be satisfied [2]. Above 1 GHz, absorbers are fabricated in the form of pyramidal (standard, twisted, or hollow), wedge, convolved, or multilayered geometries, the pyramidal shape being the most common one [5]. Pyramidal absorbers are fabricated in different lengths, depending on the lower limit of the operating band. Specifically, with the optimized carbon loading, the one and eight wavelength absorber's reflective is around -33 dB and -51 dB [5]. Also, for mechanical reasons, the base-to-height ratio is about 2.5 [1]. The product is commonly black after fabrication and is painted with blue latex to improve light reflectance. The tips are retained unpainted to prevent absorption degradation in the millimeter-wave band. The measured data do not seem to support such a common practice, and the whole absorbers should be unpainted to achieve improvements at the millimeter band [35]. Moreover, pressure-sensitive adhesives can be used for the installation, and fire-retardant chemical loading is used to meet the current fire retardancy requirements [5].

At the low-frequency limit, when the period of the array is small compared to the wavelength, homogenization of the transversely periodic structure in **Figure 2** with a transversely uniform medium with anisotropic permittivity and permeability can be used for the analysis. Thus, the longitudinal and transverse components of the constitutive parameters can be approximated as [36]:

$$\varepsilon_z = (1 - g)\varepsilon_0 + g\varepsilon_a \quad (7)$$

$$\mu_z = (1 - g)\mu_0 + g\mu_a \quad (8)$$

$$\varepsilon_t = \varepsilon_0 \left[1 + g \frac{2(\varepsilon_a - \varepsilon_0)}{(1 + g)\varepsilon_0 + (1 - g)\varepsilon_a} \right] \quad (9)$$

$$\mu_t = \mu_0 \left[1 + g \frac{2(\mu_a - \mu_0)}{(1 + g)\mu_0 + (1 - g)\mu_a} \right] \quad (10)$$

where the subscripts t and a respectively indicate the transverse component and parameters referring to the absorbing material. Also, the parameter g is defined based on the pyramid length L and the distance of the layer from the tip z as $g = (z/L)^2$. The accuracy of the aforesaid equations for practical materials is around 5% [36]. In another low-frequency approach, the pyramid is divided into multiple layers

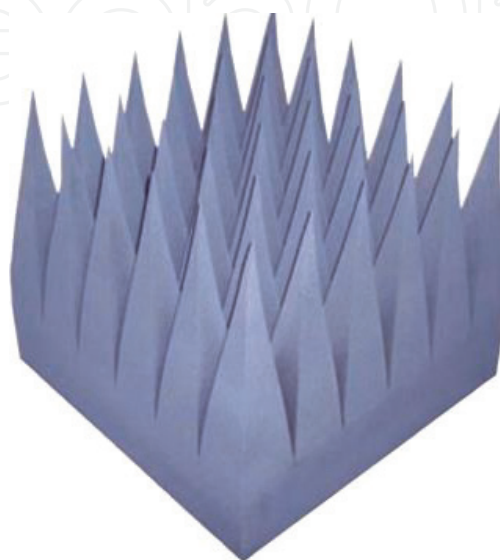


Figure 2.

The schematic view of the pyramidal absorber [24] (The photo used with permission of ETS-Lindgren).

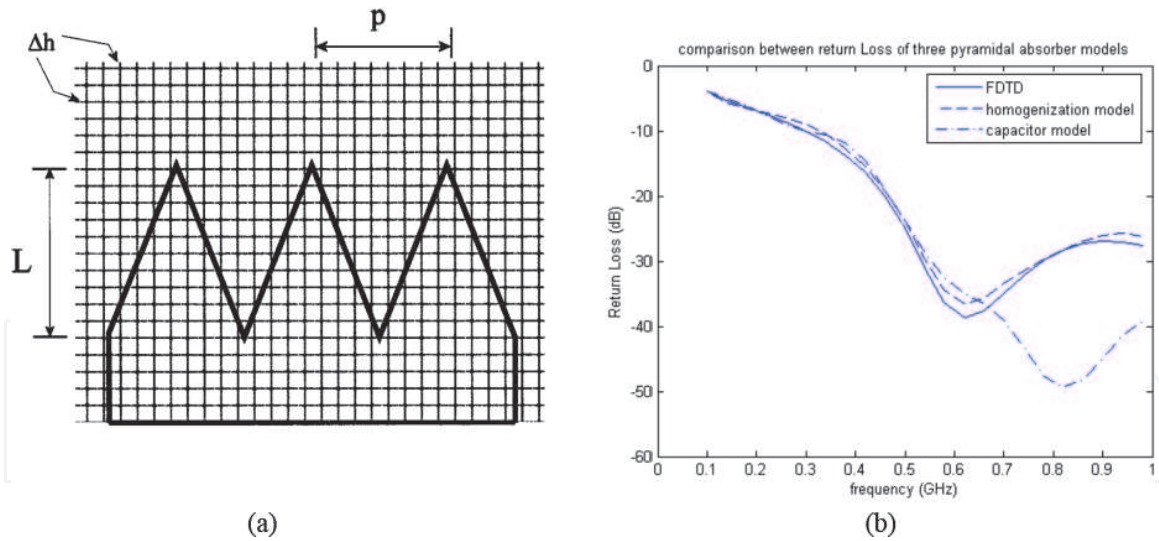


Figure 3. (a) Spatial meshing of the pyramidal absorber for its analysis based on FDTD and (b) its return loss in comparison with the homogenization model and capacitor model ([16], reproduced courtesy of The Electromagnetics Academy).

with label i , and then, each layer is approximated with the permittivity and permeability of [37]:

$$\epsilon_{ieq} = (1 - K_i) + \frac{K_i \epsilon_a}{K_i + (1 - K_i) \epsilon_a} \quad (11)$$

$$\mu_{ieq} = (1 - K_i) + \frac{K_i \mu_a}{K_i + (1 - K_i) \mu_a} \quad (12)$$

where the parameter K_i represents the normalized area of the absorber in the i th layer. The transmission-line model can be used to calculate the multiple reflection and transmissions coefficients by starting from the metal-backed bottom layer. Note that surface fraction models have been used in another homogenization approach, called the synthesized capacitance model [38].

Apart from low-frequency approximate techniques, various full-wave numerical and quasi-analytical methods such as the finite element method (FEM), the integral-equations-based method of moments (MoM), and the FDTD technique can be used for the pyramidal absorber analysis. In this regard, time-domain methods are more reasonable choices due to the wideband nature of the problem [39]. Thus, for accurate wideband modeling of pyramidal absorbers, the FDTD method can be used. The required spatial meshing for this approach is illustrated in **Figure 3(a)**, and its return loss in comparison with the homogenization model and capacitor model is included in **Figure 3(b)**, where good agreement with the former approach is attained [16].

Importantly, the bi-static or off-angle behavior of the absorbers is an important factor affecting the validity of the indoor facilities for RE/RI measurements. Therefore, polynomial approximations are proposed to predict reflected energy from pyramidal RF absorbers in different incident angles [1, 40, 41].

2.3 Hybrid absorbers

To design an absorber covering the sub-GHz and GHz frequencies, hybrid absorbers, simultaneously exploiting both technologies mentioned above, are proposed. Hybrid absorber design is not just putting the pyramidal absorbers above the

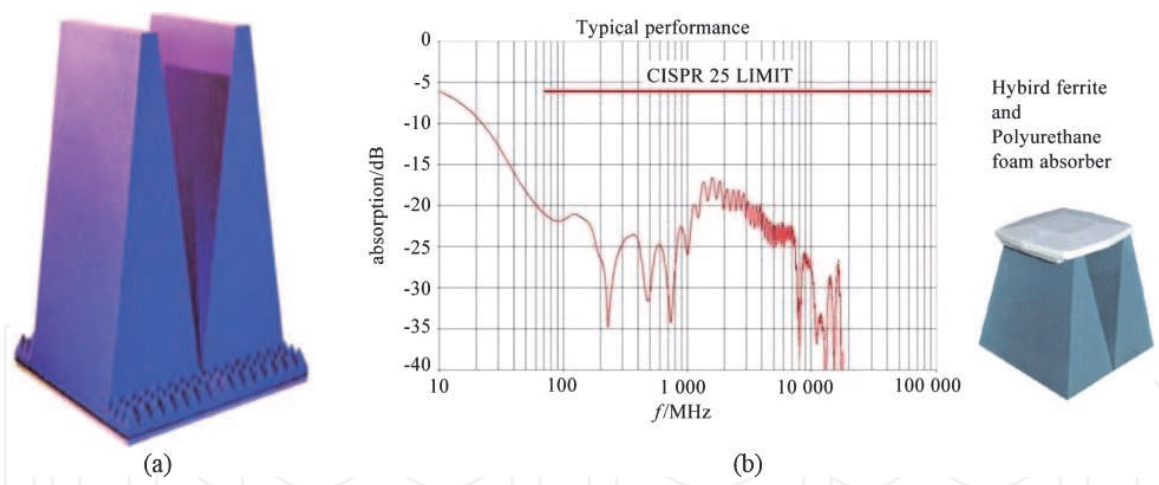


Figure 4.

(a) Hybrid absorber designed by controlling the amount of carbon loading and using pyramid's tip truncation [24] and (b) typical reflectivity of a hybrid absorber at low-frequencies [3] (The photos used with permission of ETS-Lindgren).

ferrite tiles [42]. Adjusting the carbon loading of the dielectric pyramidal absorbers, making the pyramidal absorbers hollow, or using shaped coatings of lossy paint are some solutions to improving the impedance matching of hybrid absorbers. Also, the absorption degradation due to a lower amount of carbon material is compensated by truncating the pyramid's tip, and some small-sized elements are included to improve the high-frequency performance, as in **Figure 4** [24]. Moreover, using a matching layer between the pyramidal and ferrite absorbers is another method. Fourier analysis and the mode-matching technique have been used to analyze this absorber efficiently [17]. Note that when several thousands of hybrid absorbers with complex material parameters are used in the facility design, a thin-surface impedance sheet with the same reflectivity can be used to provide time and memory efficiency instead of simulating the hybrid absorber. For this purpose, the reflectivity of the absorber must be approximated by optimizing the material parameters and thicknesses in the equivalent multilayered model [43, 44]. Modeling the absorber arrays as multilayered media through homogenization aids in analyzing the chambers using Green's function of the layered media [45].

2.4 Millimeter-wave absorbers

With the development of fifth-generation (5G) communication technology utilizing massive multiple-input multiple-output (MIMO) phased array antennas for high-speed communication, the use of millimeter-wave absorbers (30–300 GHz) with high-power handling capability is necessary for test facilities [46–48]. Convoluted (egg-carton) absorbers with the typical absorption of 50 dB at normal incidence at 30 GHz are primarily useful in millimeter-wave bands [1, 2]. The manufacturers also suggest convoluted absorber in this frequency spectrum because of tolerating wide incident angles and suggest ordering them without paint [49]. Moreover, pyramidal structures with vent holes and heat sinks are proposed, and associated power-handling capability is analyzed using multi-physics simulations [50]. Also, a millimeter-wave metamaterial absorber bandwidth is widened by embedding one of the resonators inside another in the unit cell. The device is fabricated by a standard optical photolithography process, and the measurement is done by a custom-made spectrometer, as shown in **Figure 5** [51]. Furthermore, the optical transparency requirement for some special EM protections, demanding large

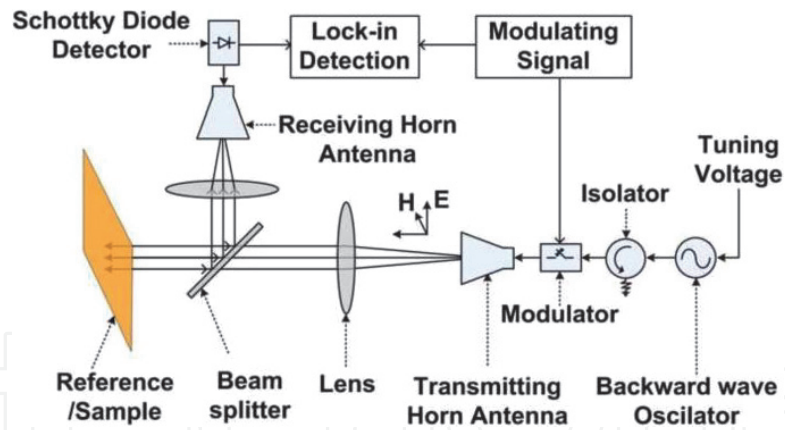


Figure 5. Measurement setup of the millimeter-wave absorber ([51], reproduced courtesy of The Electromagnetics Academy).

light transmittance and high absorptivity, can also be satisfied [52–54]. As a final note, naturally thin and transparent graphene material has great potential in the millimeter-wave absorber design [55].

3. Conclusions

Depending on the frequency range of interest, different absorber types have been commonly used for EMC applications. For the sub-1 GHz range, the magnetic losses of unbiased ferrite tiles or grids are the main mechanism for electromagnetic absorption. Moreover, pyramidal absorbers fabricated by organic, electric, or magnetic materials have been exploited frequently in microwave frequencies. Considering the coverage of both spectrums mentioned above, efficiently designed hybrid absorbers, using both technologies simultaneously, have been proposed. They have been achieved by controlling dielectric pyramidal absorbers' carbon loading and tip truncation or by designing a matching layer between the two absorbing sections. Finally, in the millimeter-wave regime, metamaterial absorbers have been proposed for providing the measurement setups of ever-growing high-frequency applications, such as 5G communication. The one-atom-thick graphene material also has great potential for this purpose.

Acknowledgements

The author would like to thank ETS-Lindgren Company for guiding through the use of necessary sources.

Conflict of interest

The authors declare no conflict of interest.

IntechOpen

IntechOpen

Author details

Shiva Hayati Raad

Department of Electrical and Computer Engineering, Tarbiat Modares University,
Tehran, Iran

*Address all correspondence to: shiva.hayati@modares.ac.ir

IntechOpen

© 2021 The Author(s). Licensee IntechOpen. This chapter is distributed under the terms of the Creative Commons Attribution License (<http://creativecommons.org/licenses/by/3.0>), which permits unrestricted use, distribution, and reproduction in any medium, provided the original work is properly cited. 

References

- [1] Rodriguez V. *Anechoic Range Design for Electromagnetic Measurements*. Artech House; 2019
- [2] Xu Q, Huang Y. *Anechoic and Reverberation Chambers: Theory, Design, and Measurements*. United States: Wiley-IEEE Press; 2019
- [3] Rodriguez V. Automotive component EMC testing: CISPR 25, ISO 11452-2 and equivalent standards. *IEEE Electromagnetic Compatibility Magazine*. 2012;1(1):83-90
- [4] Eser S, Sevgi L. Open-area test site (OATS) calibration. *IEEE Antennas and Propagation Magazine*. 2010;52(3): 204-212
- [5] Hemming LH. *Electromagnetic Anechoic Chambers: A Fundamental Design and Specification Guide*. Wiley Interscience; 2002
- [6] Demakov AV, Komnatnov ME. TEM cell for testing low-profile integrated circuits for EMC. In: 21st International Conference of Young Specialists on Micro/Nanotechnologies and Electron Devices (EDM). Chemal, Russia: IEEE; 2020. pp. 154-158
- [7] Sittakul V, Hongthong S, Pasakawee S. Design and analysis of GTEM cell using the ferrite-tile and pyramid absorbers for EMC Test in National Institute of Metrology (Thailand). In: *IEEE Conference on Antenna Measurements & Applications (CAMA)*. Chiang Mai, Thailand: IEEE; 2015. pp. 1-4
- [8] Sahraei A, Aliakbarian H. On the design and fabrication of a large GTEM cell and its challenges. *IEEE Electromagnetic Compatibility Magazine*. 2020;9(1):43-50
- [9] Raad SH, Atlasbaf Z. Broadband optical absorption using graphene-wrapped cross-hair/nano-rod combination. *Journal of Electromagnetic Waves and Applications*. 2021;35(3): 305-314
- [10] Raad SH, Atlasbaf Z. Broadband continuous/discrete spectrum optical absorber using graphene-wrapped fractal oligomers. *Optics Express*. 2020; 28(12):18049-18058
- [11] Raad SH, Atlasbaf Z, Zapata-Rodríguez CJ. Broadband absorption using all-graphene grating-coupled nanoparticles on a reflector. *Scientific Reports*. 2020;10(1):1-15
- [12] Dixon P. *Theory and application of RF/microwave absorbers*. In: York Avenue: Emerson & Cuming Microwave Products, Inc 2012
- [13] Orakwue SI, Onu IP. Pyramidal microwave absorber design for anechoic chamber in the microwave frequency range of 1GHz to 10GHz. *European Journal of Engineering and Technology Research*. 2019;4(10):1-3
- [14] Liu K. Analysis of the effect of ferrite tile gap on EMC chamber having ferrite absorber walls. In: *Proceedings of Symposium on Electromagnetic Compatibility*. Santa Clara, CA, USA: IEEE; 1996. pp. 156-161
- [15] Zhu Y et al. Development of millimeter-wave em absorber with homogenization theory. *SN Applied Sciences*. 2019;1(5):398
- [16] Khajehpour A, Mirtaheri SA. Analysis of pyramid EM wave absorber by FDTD method and comparing with capacitance and homogenization methods. *Progress In Electromagnetics Research*. 2008;3:123-131
- [17] Fallahi A, Enayati A. Modeling pyramidal absorbers using the Fourier modal method and the mode matching

technique. *IEEE Transactions on Electromagnetic Compatibility*. 2016; **58**(3):820-827

[18] Xu Q, Huang Y, Zhu X, Xing L, Duxbury P, Noonan J. A hybrid FEM-GO approach to simulate the NSA in an anechoic chamber. *Applied Computational Electromagnetics Society Journal*. 2017;**32**(11):1035-1041

[19] Holloway CL, Delyser RR, German RF, McKenna P, Kanda M. Comparison of electromagnetic absorber used in anechoic and semi-anechoic chambers for emissions and immunity testing of digital devices. *IEEE Transactions on Electromagnetic Compatibility*. 1997;**39**(1):33-47

[20] http://www.ets-lindgren.com/sites/etsauthor/General_Brochures/Top%2010%20Anechoic%20Absorber%20Considerations.pdf

[21] Holloway CL, Kuester EF. A low-frequency model for wedge or pyramid absorber arrays-II: Computed and measured results. *IEEE Transactions on Electromagnetic Compatibility*. 1994; **36**(4):307-313

[22] Chen Z. IEEE STD 1128-1998: IEEE recommended practice for RF absorber evaluation in the range of 30 MHz to 5 GHz. In: *IEEE Symposium on Electromagnetic Compatibility, Signal Integrity and Power Integrity (EMC, SI & PI)*, long beach CA: IEEE; 2018. pp. 1-16

[23] Tyagi SK. Development of semi-anechoic shielded chamber using ferrite-PU foam hybrids. *IETE Technical Review*. Taylor and Francis 2006;**23**(2):105-111

[24] Wiles M, Rodriguez V. Choosing the Right Chamber for Your Test Requirements. *Interference Technology USA: 2010. EMC Directory Design Guide*

[25] ETS-Lindgren. Texas; <http://ets-lindgren.com/datasheet/absorber/emc-absorbers/ferrite-tile-absorber/1002/100201>

[26] Holloway CL, McKenna P, Johnk RT. The effects of gaps in ferrite tiles on both absorber and chamber performance. In: *IEEE International Symposium on Electromagnetic Compatibility*. Symposium Record (Cat. No. 99CH36261), Seattle, WA, USA: IEEE; Vol. 1. 1999. pp. 239-244

[27] Vogt A, Kolodziej H, Sowa A. An effective solution to the problem of the ferrite tile gap effect. In: *IEEE EMC International Symposium*. Symposium Record. International Symposium on Electromagnetic Compatibility (Cat. No. 01CH37161). Vol. 1. Montreal, QC, Canada: IEEE; 2001. pp. 179-182

[28] Chen Z, Sha F. The simulation and analyzing of ferrite grids used in EMC anechoic chamber. In: *IEEE International Symposium on Microwave, Antenna, Propagation and EMC Technologies for Wireless Communications*. Beijing, China: IEEE; Vol. 1. 2005. pp. 666-669

[29] Xiong Z, Chen Z. Homogenization modeling of periodic magnetic composite structures. In: *IEEE International Symposium on Electromagnetic Compatibility & Signal/Power Integrity (EMCSI)*. Washington, DC, USA: IEEE; 2017. pp. 437-441

[30] Akpınar E, Erdoğan Y. The important points for determining the requirements of EMC chambers. *International Journal of RF and Microwave Computer-Aided Engineering*. 2016;**26**(4):367-372

[31] Razavi SMJ, Khalaj-Amirhosseini M, Cheldavi A. Minimum usage of ferrite tiles in anechoic chambers. *Progress In Electromagnetics Research*. 2010;**19**: 367-383

- [32] Clegg J et al. A Method of Reducing the Number of Ferrite Tiles in an Absorber Lined Chamber. EMC York, UK: IEEE; 1999
- [33] Nornikman H, Fareq M, Soh PJ, Azremi AAH, Wee FH, Hasnain A. Parametric studies of the pyramidal microwave absorber using rice husk. Available from: <http://dspace.unimap.edu.my:80/dspace/handle/123456789/33275>, 2010
- [34] Park M-J, Kim S-S. Design of wide bandwidth pyramidal microwave absorbers using ferrite composites with broad magnetic loss spectra. *Electronic Materials Letters*. 2016;**12**(5):610-614
- [35] Chen Z. Common RF absorbers evaluations in W-band (75-100 GHz). In: *IEEE International Symposium on Electromagnetic Compatibility & Signal/Power Integrity (EMCSI)*. Washington, D.C.: IEEE; 2017. pp. 1-31
- [36] Kuester EF, Holloway CL. A low-frequency model for wedge or pyramid absorber arrays-I: Theory. *IEEE Transactions on Electromagnetic Compatibility*. 1994;**36**(4):300-306
- [37] Park M-J, Choi J, Kim S-S. Wide bandwidth pyramidal absorbers of granular ferrite and carbonyl iron powders. *IEEE Transactions on Magnetics*. 2000;**36**(5):3272-3274
- [38] Anzai H, Saikawa M, Mizumoto T, Naito Y. Analysis of the pyramid electromagnetic wave absorber-an approximated model and its application of TE wave. *Electronics and Communications in Japan*. 1995; **78**(11):33-42
- [39] Holloway CL, McKenna PM, Dalke RA, Perala RA, Devor CL. Time-domain modeling, characterization, and measurements of anechoic and semi-anechoic electromagnetic test chambers. *IEEE Transactions on Electromagnetic Compatibility*. 2002;**44**(1):102-118
- [40] Rodriguez V, Barry E. A polynomial approximation for the prediction of reflected energy from pyramidal RF absorbers. In: *AMTA Proceedings*. San Diego, CA, USA: IEEE; 2016. pp. 1-6
- [41] Rodriguez V. Basic rules for anechoic chamber design: Part one: RF absorber approximations. *Microwave Journal*. 2016;**59**(1):72-86
- [42] X. Meng and W. Ying-hong, Impedance matching of compound absorber's impact on characteristic of anechoic chamber, in *IEEE-APS Topical Conference on Antennas and Propagation in Wireless Communications (APWC)*, Cape Town, South Africa: IEEE; 2012. pp. 1278-1280.
- [43] Reddy V, Kralicek P. Modeling of semi-anechoic chamber for use in automotive EMC simulations. In: *IEEE MTT-S International Microwave and RF Conference (IMaRC)*. Hyderabad, India: IEEE; 2015. pp. 93-95
- [44] Reddy V, Kralicek P, Hansen J. A novel segmentation approach for modeling of radiated emission and immunity test setups. *IEEE Transactions on Electromagnetic Compatibility*. 2017; **59**(6):1781-1790
- [45] Chen Z, Wang Y. Efficient and accurate modeling of EMC anechoic chambers using a combined discrete complex image and raytracing method. In: *15th European Conference on Antennas and Propagation (EuCAP)*. Dusseldorf, Germany: IEEE; 2021. pp. 1-5
- [46] Zhang Y, Zhu Y, Qi Y, Yu W, Li F, Liu L. High-power broadband honeycomb absorber for 5G millimeter wave chambers. In: *IEEE International Symposium on Electromagnetic Compatibility and 2018 IEEE Asia-Pacific Symposium on Electromagnetic Compatibility (EMC/APEMC)*. Suntec City, Singapore: IEEE; 2018. pp. 103-105

- [47] Chang K, Sun C. Millimeter-wave power-combining techniques. *IEEE Transactions on Microwave Theory and Techniques*. Suntec City, Singapore, IEEE; 1983;**31**:91-107
- [48] Xiaoyong L, Shuyun H, Mengjun W, Yan L, Erping L. A compact ultra-wideband polarization-insensitive metamaterial absorber at 5G millimeter wave band. In: *IEEE MTT-S International Conference on Numerical Electromagnetic and Multiphysics Modeling and Optimization (NEMO)*. Hangzhou, China: IEEE; 2020. pp. 1–4
- [49] <https://www.laird.com/products/microwave-absorbers/microwave-absorbing-foams/eccosorb-cv>.
- [50] Gong P, Liu L, Qi Y, Yu W, Li F, Zhang Y. Multiphysics analysis of millimeter-wave absorber with high-power handling capability. *IEEE Transactions on Electromagnetic Compatibility*. 2017; **59**(6):1748-1754
- [51] Singh P, Kabiri Ameri S, Chao L, Afsar MN, Sonkusale S. Broadband millimeterwave metamaterial absorber based on embedding of dual resonators. *Progress In Electromagnetics Research*. 2013;**142**:625-638
- [52] Xue B, Hu Y, Wu B, Chen L, Zhang W. A wideband transparent absorber for microwave and millimeter wave application. In: *Sixth Asia-Pacific Conference on Antennas and Propagation (APCAP)*. Xi'an, China: IEEE; 2017. pp. 1–3
- [53] Yin Z et al. Optically transparent and single-band metamaterial absorber based on indium-tin-oxide. *International Journal of RF and Microwave Computer-Aided Engineering*. 2019;**29**(2):e21536
- [54] Lai S, Wu Y, Wang J, Wu W, Gu W. Optical-transparent flexible broadband absorbers based on the ITO-PET-ITO structure. *Optical Materials Express*. 2018;**8**(6):1585-1592
- [55] Wu B et al. Experimental demonstration of a transparent graphene millimetre wave absorber with 28% fractional bandwidth at 140 GHz. *Scientific Reports*. 2014;**4**(1):1-7